ELSEVIER

Surface Science 494 (2001) 1–20

SURFACE SCIENCE

www.elsevier.com/locate/susc

Investigation of vinyl phosphonic acid/hydroxylated α-$Al_2O_3(0001)$ reaction enthalpies

L.G. Hector Jr. [a], S.M. Opalka [a], G.A. Nitowski [a], L. Wieserman [a], D.J. Siegel [b], H. Yu [c], J.B. Adams [c,*]

[a] *Alcoa Technical Center, Alcoa Center, PA 15069-0001, USA*

[b] *Department of Physics, University of Illinois at Urbana-Champaign, 1110 West Green St, Urbana, IL 61801, USA*

[c] *Department of Chemical and Materials Engineering, Arizona State University, Tempe, AZ 85287-6006, USA*

Received 26 February 2001; accepted for publication 12 June 2001

Abstract

The eleven ion vinyl phosphonic acid (VPA) molecule consists of a phosphorus ion that serves as a cationic anchor for two electron-rich functional groups, viz., a tripodal oxygen-rich base and vinyl hydrocarbon tail. Recent inelastic tunneling experiments have implied that VPA binds in a tridentate coordination though its base leaving the vinyl tail free to react with a resin in adhesive bonding applications. Using first-principles total energy calculations, the reaction enthalpies for bonding of a single VPA molecule to selected threefold sites on hydroxylated α-$Al_2O_3(0001)$ are investigated. Tridentate, bidentate and unidentate coordinations, both with and without liberated water molecules, are examined to determine if the tridentate coordination is favored over the others and the extent to which the VPA molecule is sensitive to surface site geometry. The electron localization function is used to examine the extent of covalent character between the P–O bonds that anchor the VPA fragment to the oxide surface. Some comments on the entropic contributions of the VPA and H_2O molecules to the binding energetics are offered, along with a discussion of the effects of H_2O placement on the oxide surface and aluminum alloying agents.

Keywords: Aluminum oxide; Tunneling; Surface chemical reaction

1. Introduction

Aluminum alloy surfaces consist of a natural oxide layer that will not form a stable bond with polymeric resins [1–3]. These surfaces are commonly treated with chromate conversion coatings that facilitate binding with a resin: this provides a convenient mechanism for adhesive bonding of metal sheets [4]. The presence of Cr(VI) ions in the treatment solutions presents both health and environmental problems. An alternative treatment that eliminates the undesirable aspects of chromate Organophosphorus acids are also beneficial for corrosion inhibition, painting, and lamination [5–9].

Vinyl phosphonic acid (VPA) ($H_3C_2P(O)(OH)_2$), is a representative organophosphorus acid that has received some attention in the experimental literature [2]. A schematic of a VPA molecule is shown

* Corresponding author. Tel.: +1-9653316; fax: +1-9650037.
E-mail address: jim.adams@asu.edu (J.B. Adams).

0039-6028/01/$ - see front matter
PII: S0039-6028(01)01387-5

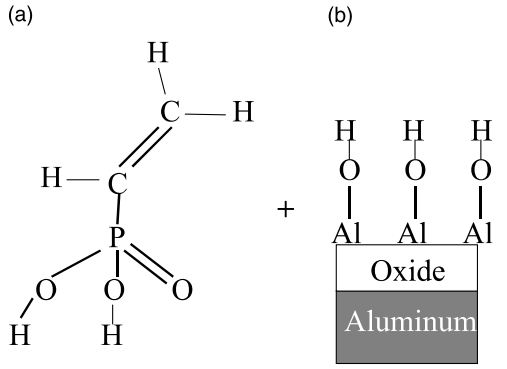

Fig. 1. VPA/oxide reaction products: (a) VPA molecule, (b) hydroxylated α-Al_2O_3(0 0 0 1).

in Fig. 1a. The VPA molecule contains a phosphorus ion that serves as a cationic anchor for two electron-rich functional groups, viz., a tripodal "oxygen-rich" base and vinyl hydrocarbon tail.

In Refs. [1,2], Fourier transform-infrared spectroscopy (FT-IR) was used to determine the vibrational modes of a VPA molecule. However, due to the small cross-section of the molecule, routine FT-IR reflection techniques did not provide detailed spectra of the species adsorbed onto hydroxylated aluminum oxide. To study binding configurations of the adsorbed species, inelastic tunneling spectroscopy (IETS) [10] was used by these same authors. The IETS spectrum of VPA on hydroxylated aluminum oxide was found to exhibit a strong C=C stretching vibration at 1613 cm^{-1}, and a band that is attributed to the asymmetric CH_2 stretch at 3073 cm^{-1}. This implied that the vinyl group did not participate in bonding with the oxide surface. The presence of a band assigned to the PO_3^2 deformation mode (573 cm^{-1}) and the absence of the P=O stretch at 1125 cm^{-1} in the IETS spectrum of the reacted VPA species implied that VPA reaction with the oxide surface resulted in a tridentate coordination. Hence, the reacted species serves as a molecular cap that may inhibit the migration of corrosion species into the oxide surface, while leaving the vinyl group accessible to react with resins (e.g. amines). The tridentate coordination is not unique to the VPA molecule as this coordination has been noted for other phosphonic acids [11].

The IETS work led to the conclusion that each VPA molecule binds to aluminum oxide as a consequence of acid–base reactions with the oxide surface. These involve reactions between the deprotonated hydroxyl groups and the phosphoryl oxygen ion (i.e. doubled bonded with the phosphorus ion) of the VPA molecule, and the hydroxyl groups on the aluminum oxide surface. A schematic of the oxide surface is shown in Fig. 1b.

Each chemisorbed VPA species contains three symmetrical phosphorus–oxygen–aluminum bonds in a tridentate coordination. A schematic of a proposed condensation reaction pathway that leads to a tridentate coordination is shown in Fig. 2a–d. Note that "R" represents the vinyl group ($CHCH_2$), and the dotted lines represent hydrogen bonding. In Fig. 2a, the VPA molecule interacts with oxide OH groups (which are Lewis bases) through hydrogen bonding. Fig. 2b shows an intermediate

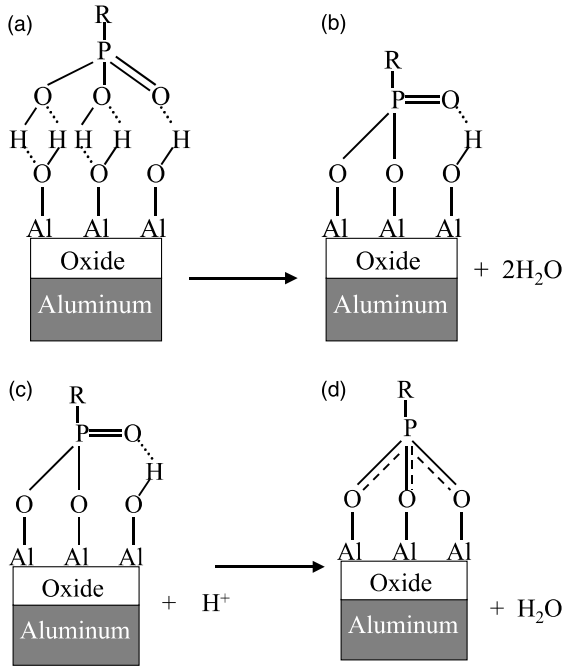

Fig. 2. VPA/oxide reaction pathway, acid–base condensation reactions of hydrogen-bonded structure: (a) VPA H-bonded to hydroxylated surface, (b) condensed VPA complex. VPA/oxide reaction pathway leading to tridentate coordination: (c) acid-promoted condensation reaction, (d) resonance-stabilized phosphonate complex (tridentate coordination).

structure in which two H_2O molecules have been liberated through reaction with two VPA legs and two surface hydroxyl groups. The phosphoryl oxygen begins interaction with a third oxide surface OH group. Addition of a H ion in Fig. 2c leads to the liberation of a third H_2O molecule, and finally the tridentate coordination suggested by Fig. 2d. The dashed lines in Fig. 2d suggest a resonance stabilized structure [12] in which the phosphorus ion is tetrahedrally coordinated. [1] The reaction functionalizes the aluminum oxide surface by leaving the vinyl group accessible to react with a polymeric resin.

In the present work, we used the plane-wave density functional theory (DFT) code VASP to calculate the reaction enthalpies associated with a series of proposed VPA bonding coordinations on hydroxylated α-Al_2O_3(0 0 0 1). [2] Following the spirit of the experimental results from the referenced IETS work, we designed a set of bound structures, such as that shown in Fig. 2d, that allowed us to explore the possibility of predicting an energetically favorable tridentate coordination. We also examined selected bidentate and unidentate coordinations, and considered the importance of water molecules liberated through condensation on the reaction enthalpies. [3] One of the key aspects of this work was to test whether or not tridentate coordination requires that the VPA molecule be sensitive to the geometry and local electronic structure of the surface site to which it binds. The structure of the VPA tripodal base, which must be such that the phosphorus ion is tetrahedrally-coordinated (or very nearly so) both before and after tridentate bonding to the oxide surface, is indicative of a corresponding threefold (or triangular-shaped) oxide surface site geometry, irrespective of the long range structure of the oxide surface. For this reason, we chose α-Al_2O_3(0 0 0 1) as our surface. The change in total distance between the phosphorus ion (in the bound VPA fragment) and the underlying Al ion within the relaxed oxide slab that lies along the centroidal axis through each binding site was calculated. This issue, which includes possible electrostatic interactions between these two ions, is of special interest due to the variety of metallic alloying agents used in aluminum alloys [16]. The local electronic structure of VPA in a tridentate coordination was examined with the electron localization function (ELF).

The rest of the paper is organized as follows. In Section 2, we outline the computational methodology that was used to relax each structure and subsequently calculate the associated reaction enthalpies. In Section 3, we consider VPA conformations and associated energetics. The bond character in a relaxed VPA molecule is addressed with the ELF. In Section 4, we consider the hydroxylated α-Al_2O_3(0 0 0 1) surface that was used for all bound structures. In Section 5, the calculated reaction enthalpies of relaxed tridentate, bidentate and unidentate VPA/α-Al_2O_3(0 0 0 1) bound structures, and the structures themselves, are individually examined and pertinent comparisons are made. To reveal some detail of adsorbate/surface bond character, an ELF analysis was conducted on a relaxed tridentate coordination, in which a single H_2O molecule liberated through condensation subsequently adsorbed at an adjacent surface site. Finally, some comments on the entropic contributions of the VPA and H_2O molecules to the binding energetics are offered, along with a discussion of the effects of H_2O placement on the oxide surface and aluminum alloying agents.

2. Computational methodology

All reaction enthalpy calculations reported in this paper are based upon density functional theory [17,18] with a plane wave basis set [19,20]. Solution of the Kohn–Sham equations was achieved using the Vienna ab initio simulation package (VASP),

[1] There is no equivalent adsorbed species involving a phosphorus ion bound to a base containing four oxygen ions and the vinyl tail.

[2] The natural oxide on aluminum sheet surfaces is very complex and we made no attempt to simulate what is the substantially amorphous, mixed-oxide surface structure common to many aluminum alloys [3,13,14].

[3] One of the distinguishing features of liquid–solid surface reactions is that many transition states may exist [15]. This required that we limit the number of models based upon the VPA geometry and IETS results.

which calculates the Kohn–Sham ground state via an iterative unconstrained band-by-band matrix diagonalization scheme using an optimized charge density mixing [21–23]. We initially calculated all reaction enthalpies with Vanderbilt-type ultrasoft pseudopotentials (USP) [24] to minimize the amount of computational effort in the relaxations. We then proceeded to refine the enthalpies by repeating all relaxations on both the reaction products (or bound) structures, and the isolated reactants/products (VPA, α-Al_2O_3(0 0 0 1), H_2O), using pseudopotentials generated with the projector-augmented wave (PAW) method originally proposed by Blöchl [25]. When compared to conventional pseudopotentials, the PAW method has the advantage that the exact shapes of the valence wavefunctions are taken into account: this represents an improvement in the description of transition metals (for example) [26]. Another concern we had that led to our use of the PAW pseudopotentials was the significant overlap between the USP cutoff radii for the P–O (i.e. single) bond. The cutoff radii of each PAW pseudopotential used in this work is listed in Table 1. Our choice of the PAW pseudopotentials ensured that the sum of the cutoff radii of adjacent ions in the VPA, α-Al_2O_3(0 0 0 1) surface, and bound structures would be less than reported single bond distances [27,28]. The pseudopotential cutoff values may slightly affect the P=O distance and hence the corresponding reference energies might be in error by a small amount. This would lead to a small constant shift of the absorption enthalpies, but would not affect the relative ranking of the reaction enthalpies for the different models we considered. We note that the reaction enthalpies calculated with the USP differed from those calculated with the PAW by 5–11%: the breadth of this range was due to the different coordinations (i.e. tridentate, bidentate, unidentate) we considered for a bound VPA fragment on α-Al_2O_3(0 0 0 1). The calculated reaction enthalpy trends in going from one coordination to the next were the same for both PAW and USP pseudopotential sets.

Table 1
Cutoff radii of VASP PAW GGA pseudopotentials

Pseudopotential	O	P	H	C	Al
Cutoff radius (Å)	0.58	1.01	0.42	0.58	1.01

Since VASP uses periodic boundary conditions, all structures were embedded in a periodic supercell. For calculations on surfaces, a 2×2 periodic repeat unit of the surface was embedded parallel to the *XY* plane of the supercell. The cell dimensions of $8.22 \times 9.50 \times 20.00$ Å^3 ensured a minimum vacuum distance of 10 Å for each of the VPA/α-Al_2O_3(0 0 0 1) structures. Care was taken to make sure that the final reaction enthalpies were in all cases independent of the vacuum distance and the cell size. Isolated molecules (VPA, water) were placed in the same cell used for α-Al_2O_3(0 0 0 1). Plane wave cutoff and *k*-point sampling tests were conducted on the reaction enthalpy of an unrelaxed bound structure to determine the optimum settings for these quantities for all ensuing calculations. All calculations were conducted with a plane wave energy cutoff of 700 eV. Sampling of the irreducible wedge of the Brillouin zone (IBZ) was performed with a regular Monkhorst–Pack grid of special k points (4 total) [29]. Ground state atomic geometries were obtained by minimizing the Hellman–Feynman forces using a combination of the conjugate gradient and quasi-Newton algorithms [21,30], until the total force on each movable ion was 0.05 eV/Å or less. We conducted all of our calculations using the gradient-corrected functional (GGA) of Perdew and coworkers [31, 32]. The dipole moment for each bound coordination was calculated along the direction orthogonal to the surface. The corresponding enthalpy was then corrected by taking the difference between the monopole, dipole, and quadrupole in the cell and the same dipole placed in a cell with the corresponding lattice vector going to infinity.

3. Vinyl phosphonic acid molecule

3.1. Structure and energetics

Two views of a relaxed VPA molecule along with relevant bond distances are shown in Fig. 3. The tripodal base of the molecule consists of a single P ion, with a +5 valence, two hydroxyl

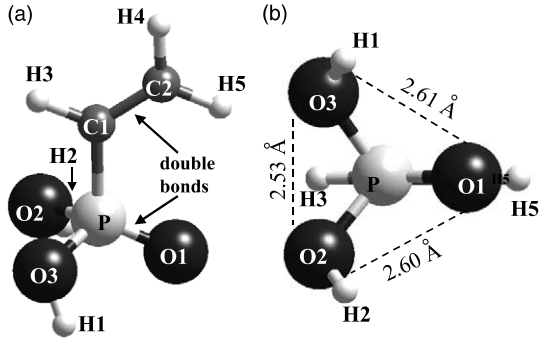

Fig. 3. Relaxed VPA molecule: (a) vinyl group and tripodal base, (b) view from underneath tripodal base.

groups, i.e., O2H2, and O3H1, and a phosphoryl oxygen, O1. Although the VPA molecule is usually represented with a double bond between the P and O1 ions, and single bonds between the P and the OH groups, a "one-and-one-third" hybrid bond between each of the P and O ions provides a more realistic description of the tripodal base structure. The H ions move (albeit slowly) between the base O ions forming equivalent tautomers, and thus the hybrid bond scenario better represents the time-averaged view of these structures [33]. The P–O bonds can be visualized as three "legs" of a tripodal base, as shown in Fig. 3b, for which the VPA molecule in Fig. 3a has been rotated through 90° about the axis in and out of the page. Note that the distances listed in Fig. 3b pertain to distances between the centers of adjacent O ions in the tripodal base. As depicted in Fig. 2a–d, it is through one or more of the tripodal legs that the VPA molecule reacts with hydroxyl bridges on the oxide surface through condensation [1,2]. The vinyl portion of the molecule consists of a hydrocarbon tail containing a doubled-bonded hydrocarbon group, i.e., C1=C2. The P ion can be considered to be tetrahedrally coordinated.

We calculated the enthalpies of a series of structures that resulted from incrementally rotating the vinyl group relative to the tripodal base. The goal of these calculations was to locate the vinyl group conformation that led to a VPA structure with the lowest calculated enthalpy. The 0° conformation was defined as the conformation in which the vinyl group was positioned as shown in Fig. 4a (looking down along the vinyl group) and Fig. 4c (side view). In this conformation, the vinyl group resides in a plane that runs midway between the two P–O–H bonds in the base. The

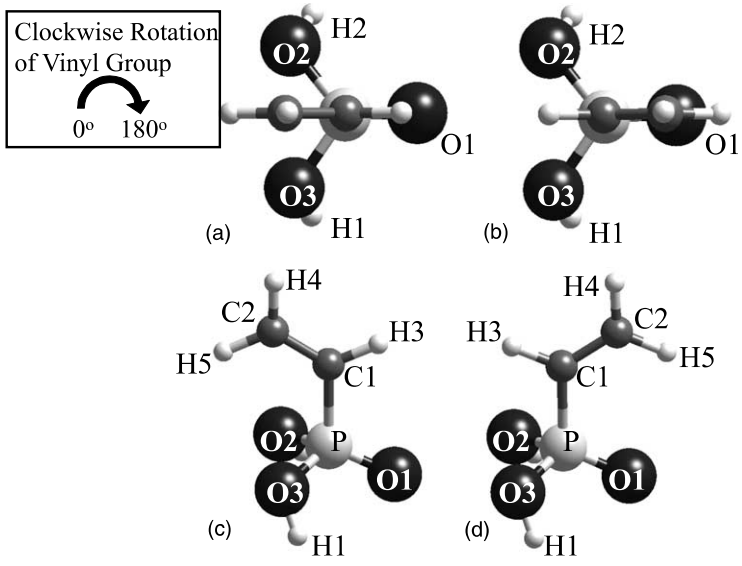

Fig. 4. (a) Top view of 0° conformation, (b) top view of 180° conformation, (c) side view of 0° conformation and (d) top view of 180° conformation.

molecule was first relaxed in the 0° conformation. The vinyl group was then manually rotated in 15° increments in a clockwise direction (relative to a downward view of the tripodal base), from 0° to 180°. Note that the relaxed 180° conformation is shown in Fig. 4b and d. In this conformation, the vinyl group was coplanar with the phosphoryl oxygen, O1. The total enthalpy of each of the conformations between 0° and 180° was then computed. We found that the 0° conformation had the highest predicted enthalpy, −63.68 eV, and that the 180° conformation had the lowest enthalpy, −63.79 eV. The 180° conformation corresponds to that predicted in Ref. [34] as being the most energetically favorable conformation for the VPA molecule. Tables 2 and 3 compare VPA bond-lengths and angles for the 180° conformation with available results in Ref. [34] based upon second-order Møeller–Plesset perturbation theory. Note that the comparisons indicate reasonable agreement between the two methodologies.

3.2. Vinyl phosphonic acid molecule bond character

The ELF, which was originally proposed in Ref. [35], is a novel graphical means for analyzing electron localization in atoms, molecules, and solids [36–39]. It is especially useful for distinguishing between regions of space where charge is localized (as in a covalent bond) or diffuse (as in a free electron gas metal such as aluminum). The ELF is a dimensionless number that ranges from 0 to 1, with specific ranges that imply the following bond characteristics:

$$\begin{cases} 0.85 \leqslant \mathrm{ELF} \leqslant 1.0: & \text{Electron localization (covalent)} \\ 0.5 \leqslant \mathrm{ELF} < 0.85: & \text{Electron delocalization (metallic)} \\ 0.0 \leqslant \mathrm{ELF} < 0.5: & \text{Minimal electron density} \end{cases} \tag{3.1}$$

Fig. 5a shows isosurfaces on the VPA molecule in the 0° conformation (see Fig. 4c) for which the ELF = 0.85. Note that the ions in the VPA molecule are color-coded as follows: red = O, green = P, white = C, and blue = H. Covalent bonds between C1=C2 and C1–P (where we have used the notation introduced in Fig. 3) are denoted by the grey lobes between these ion pairs. The region of charge localization between C1=C2 consists of π bonds, and that between the C1–P ions is a single σ bond. Two of the P–O bonds (i.e. phosphorus bound to the two hydroxyl legs) also exhibit some degree of covalency, which is suggested by the partial lobe geometry of the localized electron isosurface Fig. 5a. However, the P=O shows no such covalency in Fig. 5a as there is no localization along the P–O bond.

Fig. 5b is an ELF contour plot and corresponding scale for the molecule shown in Fig. 5a. We have elected to examine the ELF in the plane that bisects the two base hydroxyl groups in order to capture the ELF distribution around the phosphoryl oxygen. There are three blue regions within the contour plot, two three-sided lobes in the vinyl group, and a small, nearly circular patch surrounded by the asymmetrically-shaped yellow lobe (with one flat side) at the lower left of the molecule. To picture where the ions shown in Fig. 5a would lie within the contour plot in Fig. 5b, one would simply drag the molecule in Fig. 5a on top of the plot in Fig. 5b so that the ions lie on top of the letters corresponding to their names. It is important to emphasize that since we are using

Table 2
Distances between adjacent VPA ions in Fig. 3a

Bond	Ref. [34] (Å)	Present (Å)
C1=C2	1.34	1.33
C1–P	1.78	1.79
P=O1	1.40	1.47
C2–H4(H5)	1.08	1.09 (1.09)
P–O2(O3)	–	1.62 (1.62)

Table 3
Angular distances between VPA ions in Fig. 3a

Bond	Ref. [34]	VASP PAW (GGA)
C2=C1–P	119.90°	123.3°
C1–P=O1	116.90°	117.4°
P–O3–H1	–	112.1°
P–O2–H2	–	111.3°
O1–P–O2(O3)	–	114.5° (115.8°)
O2–P–O3	–	102.7°

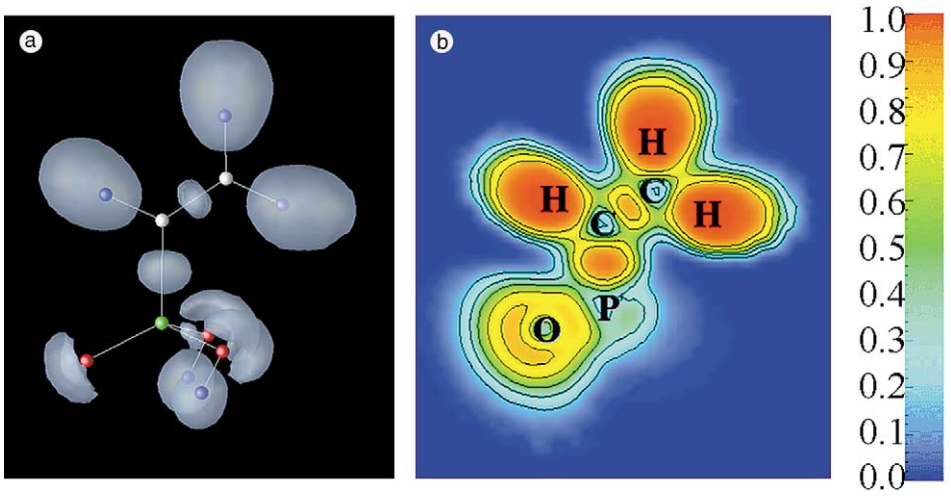

Fig. 5. Plots of electron localization function for VPA: (a) isosurface at 0.85, (b) contour plot.

pseudopotentials to account for the atomic nucleus and core electrons, there is no physical significance to the data within these regions, and the ELF typically assumes a low value there. Hence, the locations of the C, P, and O ion cores are imaged as regions of very low ELF. That corresponding to the P ion has assumed a dark blue color just beyond the flat-end of the yellow lobe surrounding the phosphoryl oxygen. The region of charge localization between the two C ions in the vinyl group is represented by the oval-shaped (orange within yellow) region between the two three-sided lobes. Charge localization between the C1 and P ions is represented by the quasi-circular orange-red region above the blue contours surrounding the P ion core. Note that there is substantial electron localization about the H ions in the vinyl group, as evident from the three oval-shaped red regions at the top of the contour plot in Fig. 5b.

4. Hydroxylated α-Al_2O_3 (0001)

The natural oxide on aluminum, which is predominantly amorphous [4], consists of AlO_4 tetrahedra with a very small number of AlO_6 octahedra [40]. In addition, the near surface oxide composition can be strongly affected by the concentration of alloying agents that have diffused from the bulk. Transition aluminas, such as γ-Al_2O_3, may also be present in addition to hydroxylated structures such as pseudoboehmite [3]. A common alloying agent is magnesium: this ion diffuses in large quantities to aluminum surfaces [41]. During thermomechanical processing of magnesium-bearing alloys, the aluminum oxide surface layer can be reduced by Mg^{+2} ions: mixed phases of cubic MgO and $MgAl_2O_4$ are usually formed [42,43]. In order to avoid difficulties with having to simulate an amorphous surface with a possible mixed-oxide structure, we elected to examine VPA reaction to crystalline α-Al_2O_3(0001) since the geometry of this much simpler model surface was conducive to tridentate coordination.

Crystalline α-Al_2O_3, in which Al ions are octahedrally coordinated, has been one of the most extensively studied metal oxides in the electronic structure literature [44,45]. The crystal structure consists of a hexagonal close-packed array of O ions, with Al ions occupying two-thirds of the interstitial octahedral sites [3]. The structure can be viewed in either its primitive rhombohedral cell, which contains two molecular units (for a total of 10 ions), with R^6_{3d} ($R\bar{3}c$) symmetry, or in its conventional hexagonal unit cell, which contains six molecular units, or 30 ions altogether.

Prior to generating the surface for the VPA reaction enthalpy studies, we calculated the lattice

Table 4
α-Al_2O_3 bulk properties

Method	a (Å)	c (Å)	B_o (GPa)	E_{coh} (eV)
VASP–LDA	4.75	12.94	240	36.40
VASP–GGA	4.82	13.16	234	32.45
AE–LCGTO–LDA[a]	4.77	12.97	249	36.45
Experiment[b]	4.759	12.99	253[c]	32.14[d]
Experiment[e]	4.758	13.00	–	–
Experiment[f]	4.763	12.98	–	–

[a] All-electron linear combination of Gaussian-type orbitals. Ref. [53].
[b] Ref. [54].
[c] Ref. [55].
[d] Ref. [56].
[e] Refs. [57,58].
[f] Refs. [57,59].

constants, bulk modulus and cohesive energy of α-Al_2O_3 using the 10 ion primitive cell. Six k-points in the IBZ were determined to be the best choices for the calculations. The total energy was converged to within 1–2 meV per ion. The lattice constants were calculated by fitting energy vs. volume data to the Murnaghan equation [46]. The calculated properties are listed in Table 4 along with pertinent experimental references for the lattice constants [47,48,51–53], bulk modulus B_o, [49] and cohesive energy E_{coh} [50]. The lattice constants calculated with LDA (at 0 K) are closer to experimental values (at room temperature – presumably the values at 0 K would only be slightly smaller) than those calculated with GGA. For this reason, we chose to construct our α-Al_2O_3 cell with the LDA-predicted lattice constants. Note that the bulk modulus values predicted with LDA, GGA, and AE–LCGTO–LDA (at 0 K) were less than the reported experimental value (again at room temperature – presumably the values at 0 K would be slightly higher). On the other hand, the GGA-calculated value of E_{coh} was the closest of the three methods to the corresponding room temperature experimental value.

For our studies of the α-Al_2O_3(0 0 0 1) surface, we created a structure composed of $2 \times 2 \times 2$ unit cells (with each unit cell including one Al_2O_3), and cleaved it such that the top surface was terminated by O ions, and the bottom surface was terminated by Al ions (see Fig. 6). We then placed H atoms above each O ion in the top surface (12 in all). The vacuum region was 10 Å, which was sufficient to minimize interactions between the tip of the VPA fragment and the Al layers at the bottom of the next image. This distance was determined to be acceptable following a test of different vacuum distances. Note that the clean α-Al_2O_3(0 0 0 1) face terminated by a single Al layer has been predicted to be the most stable under UHV conditions [45]. However, it has been reported that the oxygen-terminated surface becomes relatively more stable through hydroxylation [54].

Previous DFT calculations which explored the depth of surface relaxation in Al_2O_3(0 0 0 1) slabs were reported in Ref. [55]. In our own calculations using VASP [56], we have found that α-Al_2O_3(0 0 0 1) must be 5–7 molecular units in depth in order to converge the surface energy by the method in [57]. Our choice of a thinner slab was based upon the fact that reaction enthalpy results in which a VPA fragment was bound to the surface of hydroxylated Al_2O_3 slabs that were five molecular units in depth were within 4–5% of those from the thinner slab. In addition, it was found that the relative ordering of our reaction enthalpy calculations as a function of binding coordination was unaffected by the Al_2O_3 slab thickness. Finally, the thinner slab allowed us to minimize computational cost without a significant sacrifice in accuracy of our calculated reaction enthalpies.

In Ref. [58], molecular dynamics calculations were used to predict that one out of every three H ions (on the average) in the surface hydroxyls will lie in the plane of the surface in order to lower the slab energy through hydrogen bonding. This observation was subsequently confirmed through additional calculations reported in Ref. [59] and experiments reported in Ref. [60]. Following Ref. [58], we constructed a hydroxylated α-Al_2O_3-(0 0 0 1) slab in which one hydrogen ion in each threefold site was rotated into the plane of the oxygen ions prior to relaxation of the slab.

A simple H_2O adsorption calculation was carried out and the adsorption enthalpy was calculated via

$$H^{ads}_{H_2O} = H_{[\alpha\text{-}Al_2O_3(0\,0\,0\,1)+H_2O]} - H_{\alpha\text{-}Al_2O_3(0\,0\,0\,1)} - H_{H_2O} \quad (4.1)$$

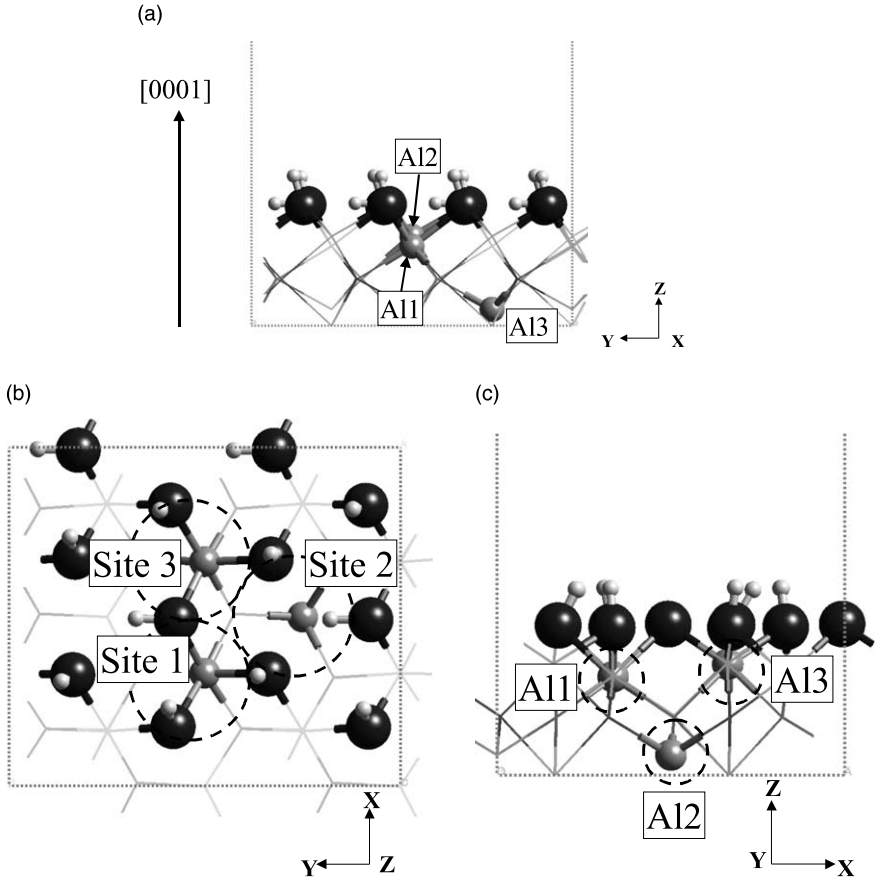

Fig. 6. α-Al_2O_3(0 0 0 1) relaxed surface structure and proposed VPA reaction sites: (a) view along *x*-direction showing H ions rotated into oxygen plane, (b) view down (0 0 0 1), (c) along *y*-direction.

where H_{H_2O} is the enthalpy of an isolated H_2O molecule, and $H_{\alpha\text{-}Al_2O_3(0001)}$ is the enthalpy of the slab (see Table 5). An adsorption enthalpy of $H^{ads}_{H_2O} = -0.42$ eV was calculated, and this lies within a reported range of energies for a moderate (mostly electrostatic) hydrogen bond [61].

Three different views of the relaxed slab are shown in Fig. 6a–c. Oxygen ions are denoted by black spheres, Al ions are denoted by gray spheres, and H ions are denoted by small white spheres. Ions lying within the top molecular unit of Al_2O_3 are shown as spheres: underlying ions lie at the intersections of the sticks. The ions in the bottom two layers of the α-Al_2O_3(0 0 0 1) slab in Fig. 6 were fixed for all calculations to simulate a bulk-effect.

Fig. 6a shows the H ions that have rotated into the topmost O ion surface plane to gain energy through hydrogen bonding. If we now rotate the slab about the *Y*-axis, we see that it has three distinct threefold sites which are encircled in Fig. 6b. We refer to these as sites 1, 2, and 3 as shown in the figure. Each site consists of hydroxyl bridges which lie at the vertices of a triangle or threefold

Table 5
Evaluation of Eq. (4.1) for H_2O adsorption enthalpy on α-Al_2O_3(0 0 0 1)

H_{H_2O} (eV)	$H_{\alpha\text{-}Al_2O_3(0001)}$ (eV)	$H_{[\alpha-Al_2O_3(0001)+H_2O]}$ (eV)	$H^{ads}_{H_2O}$ (eV)
−14.29	−316.23	−330.94	−0.42

site. The geometry of the sites makes them good candidates for reaction with the tripodal base of the VPA molecule in (see Fig. 3b, for example). Two features distinguish one site from the other. One is the distance (lying in a plane parallel to the surface) between adjacent OH bridges. For sites 1, 2, and 3, the calculations gave distances of 2.62, 2.87 and 2.74 Å, respectively. The second distinguishing feature, which is emphasized in Fig. 6c, is the location of the subsurface Al ion, which, when the surface is viewed from above, lies on the centroidal axis that cuts through the plane containing the topmost layer of O ions. Relaxation of the surface gave total distances of 1.16, 3.02 and 0.86 Å, for the site 1, 2, and 3, Al ions, respectively, beneath the surface O ions. We were especially interested in the direct distances (before and after relaxation) between these Al ions and the P ion in the bound VPA fragment, due to possible electrostatic interactions which could affect the reaction energetics and structure of the adsorbed fragment. With this in mind, it is important to emphasize that the Al ion in site 2 (i.e. Al2) was the only ion of the three site Al ions to be fixed in all of the calculations.

5. Vinyl phosphonic acid/α-Al_2O_3(0 0 0 1) structures and reaction enthalpies

5.1. Methodology for calculating reaction enthalpies

We define the reaction enthalpy, H_R, as the difference between the sum of the product enthalpies and the sum of the reactant enthalpies. The reactants consist of: (1) an isolated VPA molecule; (2) the hydroxylated α-Al_2O_3 (0 0 0 1) surface. The products consist of: (1) the oxide surface with a bound VPA fragment; (2) liquid water molecules (either bound to the surface or assumed to have joined a liquid water reference state), the number of which depends on the number of proposed VPA/α-Al_2O_3 (0 0 0 1) bonds. By definition, a negative reaction enthalpy favors the products, while a positive reaction enthalpy favors the reactants, and hence for this latter case, no reaction between VPA and the oxide surface is likely. For each model, the reaction enthalpy was converged to less than 0.05 eV per cell. It is again important to emphasize that we have not considered the activation barriers to the reactions we proposed.

When the natural oxide surface on aluminum sheet is treated with VPA, there will be many H_2O molecules liberated through condensation, thereby forming liquid water. Clearly this situation is drastically different from our models in which only a very limited number of H_2O molecules are formed through reaction between a single VPA molecule and α-Al_2O_3(0 0 0 1). We did not simulate adsorption or clustering of H_2O molecules on α-Al_2O_3-(0 0 0 1) likely to result from oxide reaction with an enormous number of VPA molecules. Instead, we attempted to make a reasonable estimate for the H_2O reaction products by referencing to the adsorbed state of H_2O on the relaxed α-Al_2O_3(0 0 0 1) surface. We therefore define the H_2O reference enthalpy by, $H^{ref}_{H_2O}$: this was calculated via

$$H^{ref}_{H_2O} = H_{[\alpha\text{-}Al_2O_3(0\,0\,0\,1)+H_2O]} - H_{\alpha\text{-}Al_2O_3(0\,0\,0\,1)} \qquad (5.1)$$

We found $H^{ref}_{H_2O} = -14.71$ eV (see Table 5).

Throughout the remainder of this section, we discuss the tridentate, bidentate, and unidentate models that we constructed for this work, and their corresponding reaction enthalpies. Since spectroscopy experiments implied a tridentate reaction coordination, we first constructed and subsequently relaxed seven models addressing the tridentate coordination which would result from the sequence of reactions shown in Fig. 2a–d. We then proceeded to examine two bidentate models, in which the two hydroxyl legs of the VPA molecule were assumed to have reacted with two hydroxyl bridges on the α-Al_2O_3(0 0 0 1), as shown in Fig. 2b. Finally, we considered three unidentate models in which only one hydroxyl leg of the VPA molecule was assumed to react with a single hydroxyl bridge on the surface (essentially resulting from one of the two condensation reactions in Fig. 2b).

5.2. Tridentate models

We examined the three distinct binding sites identified in Fig. 6b to determine which of these

sites yielded the most energetically favorable tridentate coordination. To address this issue we constructed and subsequently relaxed seven tridentate models with the method outlined above. The equations used to calculate H_R for each tridentate model are listed in Table 6. The corresponding numerical values of H_R calculated using the H_2O enthalpy from Eq. (5.1) are listed in Table 7. Also listed in Table 8 are the P–Al and P–O distances between the VPA fragment and the oxide surface in both the unrelaxed and relaxed structures. The P–Al distances in the unrelaxed structures are arbitrary since they depend only upon manual placement of the VPA fragment on the surface prior to relaxation.

Table 6
Tridentate reaction enthalpy equations

Model(s)	H_R[a]
T11,T12, T21,T22,T31,T32	$H_R = (H_{BP} + 3H_{H_2O})$[b] $- H_{\alpha\text{-}Al_2O_3(0001)} - H_{VPA}$[c]
T23	$H_R = (H^*_{BP} + 2H_{H_2O})$[d] $- H_{\alpha\text{-}Al_2O_3(0001)} - H_{VPA}$

[a] H_R = Reaction enthalpy.
[b] H_{BP} = Enthalpy of bound product, i.e. VPA fragment bound to α-$Al_2O_3(0001)$.
[c] $H^{0°}_{VPA} = -63.68$ eV, $H^{180°}_{VPA} = -63.79$ eV.
[d] H^*_{BP} includes adsorbed H_2O molecule.

Table 7
Tridentate reaction enthalpies

Model	VPA conformation	H_R (eV) $H_{H_2O} = -14.71$ eV (from Eq. (5.1))
T11	0°	+0.88
T12	180°	+0.97
T21	0°	+0.12
T22	180°	+0.13
T31	0°	+1.78
T32	180°	+1.73
T23	180°	−0.43

Table 8
P–Al and P–O distances in tridentate models

Model	P–Al (Å)		P–O (Å)[a]
	Unrelaxed	Relaxed	Relaxed
T11	2.01	2.61	1.53, 1.53, 1.59
T12	2.01	2.61	1.54, 1.56, 1.53
T21	3.62	3.62	1.56, 1.56, 1.56
T22	3.62	3.62	1.56, 1.56, 1.55
T31	1.58	2.44	1.60, 1.49, 1.62
T32	1.58	2.53	1.49, 1.62, 1.59
T23	3.64	3.64	1.56, 1.56, 1.53

[a] Clockwise relative to VPA vinyl tail.

We also examined the effect of VPA conformation on the reaction enthalpies by assuming that VPA bonded with the surface in either of the 0° and 180° vinyl conformations. The notation that we adopted to distinguish each model contains the first letter of the coordination geometry, followed by a number that identifies the surface site (shown in Fig. 6b) to which the VPA fragment was bound; the last number identifies the model number at that site. Hence, T11 pertains to tridentate coordination at site 1, model 1 in the tridentate series; T23 corresponds to tridentate coordination at site 2, model 3 in the tridentate series, and so on. We shall adopt a similar notation for the bidentate and unidentate models. For each relaxed geometry, we present views looking along $[000\bar{1}]$ and looking along the Y-axis of the cell.

The condensation reactions associated with models, T11, T12, T21, T22, T31, T32 led to the liberation of three H_2O molecules. Two H_2O molecules were liberated through a condensation reaction between the two OH legs of the VPA tripodal base and two OH bridges on the surface to form two P–O–Al bonds. Hence,

$$P[OH]_2 + 2AlOH \rightarrow P[OAl]_2 + 2H_2O \qquad (5.2)$$

The third H_2O molecule resulted from the displacement of a third surface OH bridge by the P=O leg in the VPA tripodal base. Since Fig. 2c proposes that an extra H ion is needed to complete the third H_2O molecule, we assumed (for the sake of simplicity) that a H ion was removed from an adjacent hydroxyl bridge in models T11, T12, T21, T22, T31, and T32, thereby forming the third H_2O molecule (which was also removed from the cell), leaving an exposed O ion on the oxide surface. Hence,

$$P{=}O + 2AlOH \rightarrow P[OAl] + AlO + H_2O \qquad (5.3)$$

We found that this was the quickest way to screen each of the three oxide surface sites for potentially

favorable reaction with the VPA molecule without contributions from other adsorbed reaction products. One alternative would have been to add an additional hydrogen ion to one of the hydroxyl bridges. This would presumably facilitate liberation of the third H_2O molecule through reaction with the VPA phosphoryl oxygen ion. Depending upon the availability of hydrogen, which we believe is abundant in practical applications, this would lead to a stronger binding energy of the VPA to the surface.

Clearly, the removal of a surface H ion would lead to a metastable state (the exposed O ion would most certainly react quickly with any surrounding moisture on the surface) with a corresponding reaction enthalpy that was less favorable for the products compared with that resulting from a fully hydroxylated oxide surface. As a check, we conducted spin polarized calculations and found no significant differences in the enthalpies of the tridentate structures containing a bare surface O ion. We therefore report only those results from the spin averaged calculations. Note that in all cases, the VPA phosphorus ion retained its tetrahedral coordination following relaxation.

Fig. 7 shows two different views of T12, where the condensation reaction led to direct binding between the VPA phosphorus ion and the three O ions at site 1. Fig. 7a is a top–down view along $[0\,0\,0\,\bar{1}]$. Also identified in Fig. 7a is the exposed surface O ion from which the H ion was removed to complete the third H_2O molecule. Fig. 7b is a side view along the *Y*-direction. From Table 7, the calculated reaction enthalpies due to the correction from Eq. (5.1) for an H_2O molecule is +0.97 eV: this value implies that the reactant structures are not energetically favored. Fig. 7b shows that the VPA fragment and base O ions rotated out of the plane of the surface during the relaxation. The P–O bond distances listed in Table 8 for Model T12 indicate that these bonds are nearly equivalent: this tends to support the proposed resonance stabilized tridentate coordination in Fig. 2d. The direct distance between the P ion and Al1 (as defined in Fig. 6b) changes to 2.61 Å during relaxation of the proposed bound structure. Similar observations can be made for model T11, although the reaction enthalpy of +0.88 eV was slightly lower due to the higher energy 0° VPA conformation (−63.68 eV).

Fig. 8 shows the same two views for the relaxed geometry corresponding to model T22, where the condensation reaction led to direct binding between the VPA phosphorus ion and the three O ions at site 2. The location of the exposed surface O ion relative to the VPA fragment is indicated in Fig. 8a. Note that site 2 has the lowest-lying Al ion of the three sites considered in Fig. 6 (Al2 in the figure). A comparison of Figs. 7b and 8b shows that the position of the VPA has changed very little during the relaxation that led to the geometry in Fig. 8b: the surface O ions through which the VPA phosphorus ion is bound remained within the surface plane. From Table 7, the reaction enthalpy corresponding to the adsorbed state of H_2O is +0.13 eV. This value implies that site 2 is likely to

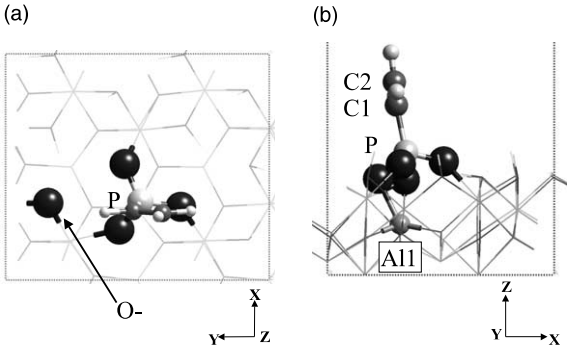

Fig. 7. Model T12, relaxed geometry: (a) view down $[0\,0\,0\,\bar{1}]$, (b) along *Y*-direction.

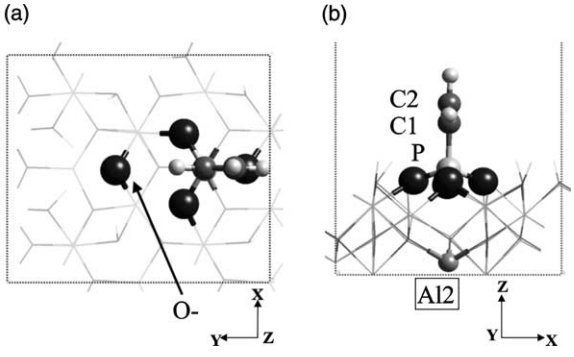

Fig. 8. Model T22, relaxed geometry: (a) view down $[0\,0\,0\,\bar{1}]$, (b) along *Y*-direction.

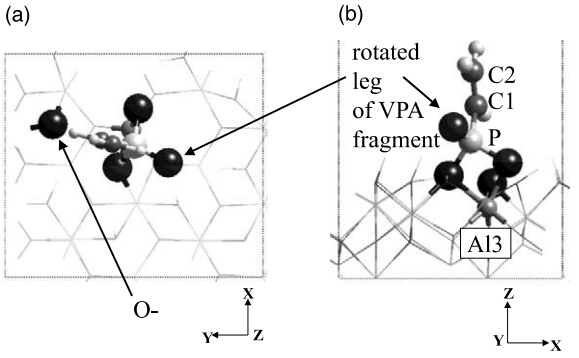

Fig. 9. Model T32, relaxed geometry: (a) view down [0 0 0 $\bar{1}$], (b) along *Y*-direction.

be more conducive to VPA binding that site 1. Note that the reaction enthalpy due to the 0° conformation (i.e. +0.12 eV) is only slightly lower than that for the 180° conformation. The P–Al distances have remained unchanged at 3.62 Å both before and after the relaxation. The P–O bond distances for both conformations at site 2 are essentially identical. Again, this supports the proposed resonance stabilized tridentate coordination in Fig. 2d.

Fig. 9 shows the same two views for the relaxed geometry corresponding to model T32, where the condensation reaction led to direct binding between the VPA phosphorus ion and the three O ions at site 3. The location of the exposed surface O ion relative to the VPA fragment is indicated in Fig. 9a. A comparison of Figs. 8b and 9b shows that one leg of the VPA fragment has detached itself from the surface to form what appears to be a bidentate structure. The P–O distances listed in Table 8 for model T32 are 1.60 Å and 1.62 Å for the two legs that connect the VPA phosphorus ions to the surface, and a 1.49 Å distance for the free P–O leg. This latter distance is close to the 1.47 Å value (listed in Table 2) for the P═O1 bond distance in the isolated VPA molecule. The +1.73 eV reaction enthalpy for T32 is the least favorable so far considered for a bound structure, and hence site 3 is unlikely to be conductive to tridentate coordination. The reason for this is probably related to the combined effects of the strain imposed upon the VPA molecule due to the required tetrahedral coordination of the P ion, and electrostatic effects due to the proximity of the centroidal Al ion (Al3 in Fig. 6c) to the VPA phosphorus ion. We note that the distances between adjacent hydroxyl bridges in the surface plane of site 3 (2.74 Å) exceeds that of the hydroxyl bridge distances in site 1 (2.62 Å) by 0.12 Å, yet the relaxed geometry shown in Fig. 7b indicates a smaller degree of tilting of the VPA fragment during relaxation. However, Table 8 shows that the P–Al distance increases during relaxation of model T32 by more than 1.0 Å. Similar observations apply for model T31 for the 0° conformation. Note that the reaction enthalpy for the 0° conformation in model T31 was +1.78 eV, which is slightly higher than its T32 counterpart.

The calculated reaction energies for models T11, T12, T21, T22, T31, and T32, listed in Table 7, show that the tridentate VPA reaction with the hydroxyl bridges in site 2 has the lowest calculated reaction enthalpies. In this site, the hydroxyl bridges in the relaxed surface are separated by 2.87 Å, the greatest distance between corresponding hydroxyl bridges in the three sites considered. In addition, the total distance between the site 2 Al ion and the P ion in the bound VPA fragment is sufficiently large enough to minimize possible electrostatic effects. Clearly, the hydroxyl bridge distances on sites 1 and 3, which are 2.62 and 2.74 Å, respectively, are closer to the (in-plane) spacing between the legs of the (relaxed) VPA base (see Fig. 3b). It appears, however, that these distances have less of an effect on the reaction enthalpies than does the proximity of the centroidal Al ion. This latter effect would need greater examination relative to the proximity of other Al ions in the oxide before a definitive conclusion is at hand. Having made these observations, we proceeded to focus the remainder of the work on the reaction energetics between VPA and site 2.

In practice, bound VPA fragments are surrounded by H_2O molecules. Since none of the previous tridentate models explored the effect of adsorbed H_2O on the oxide surface, we constructed one additional tridentate model, i.e. model T23, for this purpose. We assumed that the condensation reaction between the P═O leg and remaining site 2 hydroxyl bridge in the cell yielded an OH fragment, which upon release from the

oxide surface, adsorbed onto an adjacent hydroxyl bridge. Note that unlike the previous tridentate models, we did not remove a H ion from the surface (since we were no longer removing a third H_2O molecule from the cell). The alternative reaction to Eq. (5.3) is

$$\mathrm{P{=}O} + 2\mathrm{AlOH} \rightarrow \mathrm{POAl} + \mathrm{AlO}\cdots\mathrm{HOH} \qquad (5.4)$$

Clearly, there were many possible starting locations for the OH fragment on the surface and we could not examine all of these. Hence, we elected to place the OH fragment in the starting geometry for model T23 with the O ion at 1.0 Å directly above an H ion at site 1. The relaxed geometry for model T23 following the same two views considered in Fig. 7 is shown in Fig. 10. During the relaxation, this adsorbed hydroxyl removed a H ion from the underlying hydroxyl bridge, forming an adsorbed H_2O molecule. This is shown more clearly in Fig. 10b. These results supported the possibility of the reaction pathway given in Eq. (5.3), where a H ion was removed from an adjacent hydroxyl to form an additional H_2O molecule. The associated reaction enthalpy that was calculated from this structure was −0.43 eV (see Table 8). Although a direct comparison with model T22 involves comparing bound structures with differing numbers of bonds on the oxide surface, we observe that the adsorbed H_2O molecule contributed to a decrease in the reaction enthalpy by 0.56 eV. We anticipate that had the two additional H_2O molecules liberated from the condensation reaction at site 2 been adsorbed onto the surface, then the resulting reaction enthalpy would have been more negative than that calculated for model T23 due to contributions to the reaction enthalpy from hydrogen bonding with the surface.

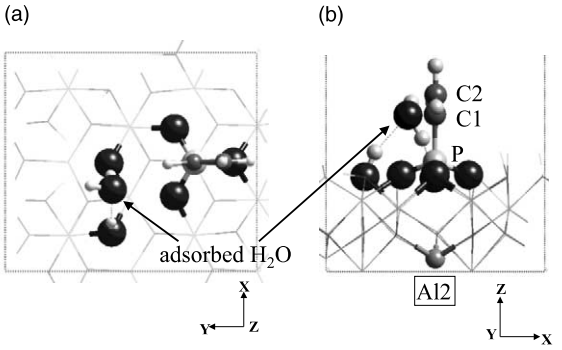

Fig. 10. Model T23, relaxed geometry: (a) view down [0 0 0 $\bar{1}$], (b) along *Y*-direction.

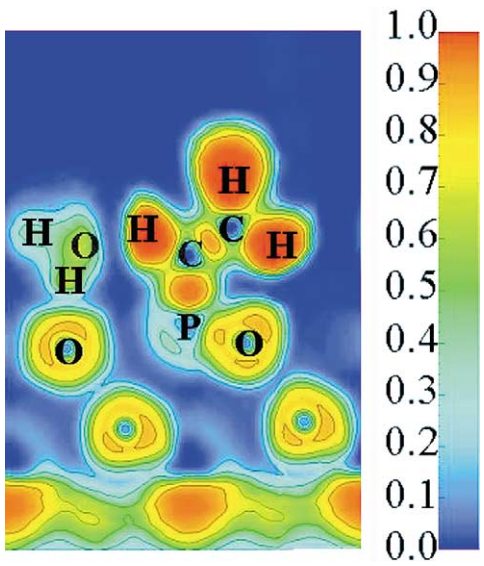

Fig. 11. Electron localization function contour plot for relaxed model T23, view along *x*-direction.

Fig. 11 is an ELF contour plot of the relaxed geometry for model T23 where ELF values are listed in the scale to the right. We elected to examine an ELF slice through one of the three P–O bonds; this slice therefore ran directly between the other two P–O bonds (analogous to Fig. 5b for the isolated VPA molecule), the details of which are not shown in Fig. 11. The bond character in the VPA vinyl group that projects upward from the surface has essentially remained unchanged following the reaction. The only difference was some reduction in pairing along two of the P–O bonds and hence a reduction in the local covalent character. Recall that in the isolated molecule (Fig. 3) there were two hydroxyl legs in the tripodal base. In the isosurface plot of Fig. 5a, we noted that there were regions of localization within the P–O bonds in these legs. In the relaxed model T23, the regions of localization (see small grey lobes in P–O–H bonds of Fig. 5a) vanished due to loss of the H ions to the condensation reaction with the sur-

face. These same bonds (now with the oxide surface) have a character that resembles the P═O bond in the isolated molecule (see Fig. 5b). In other words, the three O ions which anchor the VPA fragment to the surface all have extended regions of localization surrounding them, as indicated by the yellow lobe within which reside three smaller orange lobes (only one of these lobes is shown in Fig. 11). This suggests an ionic/electrostatic interaction for each P–O bond (or at least some type of highly polarized bonding in which the electron cloud surrounding each O ion is still intact, but strongly distorted by the presence of the P ion). The lowest portion of Fig. 11, which is blue and corresponds to the Al ions at the bottom of the oxide slab, is an artifact of the slab termination. In the interior of the oxide slab there is no delocalization. Electrons are localized mainly on the O ions as denoted by the yellow–orange rings which surround them. The rest of the interior regions are blue which corresponds to low charge density. The ionic bonding of the α-$Al_2O_3(0\,0\,0\,1)$ slab does not appear to be affected by the VPA fragment bonding at site 2. Note the ELF distribution around the adsorbed H_2O molecule to the right of the VPA fragment in Fig. 11.

5.3. Bidentate models

It can be argued that a switch from the tridentate coordination to bidentate coordination would in fact require a whole new search over the different binding sites we have identified on α-$Al_2O_3(0\,0\,0\,1)$. However, we believe that the stearic constraints on the VPA molecule are less for the bidentate and the unidentate coordinations, than for the tridentate coordination. Hence, the VPA binding in the bidentate and unidentate coordinations is likely to be less dependent upon oxide surface site geometry. Therefore, we elected to limit our investigation of both bidentate and unidentate reaction coordinations to site 2 in Fig. 6b with the VPA molecule in the 180° coordination.

Model B21 was constructed by connecting the VPA phosphorus ion to two adjacent oxide surface O ions (without their corresponding H ions) and then manually tilting the bound VPA fragment so

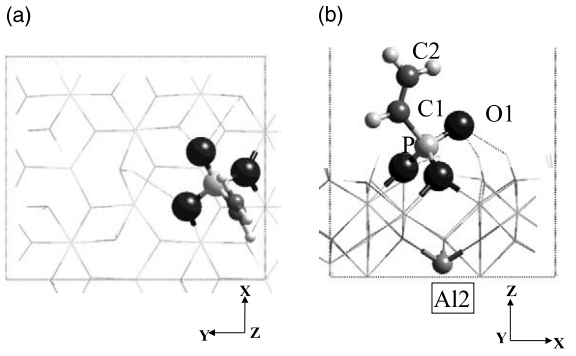

Fig. 12. Model B21, relaxed geometry: (a) view down [0 0 0 $\bar{1}$], (b) along *Y*-direction.

that the P═O leg was nearly parallel to the surface plane (as suggested in Fig. 2b). [4] Fig. 12 shows the relaxed geometry for model B21 in which legs O2H2 and O3H1 of the VPA molecule shown in Fig. 3 reacted with two OH bridges in site 2 of Fig. 6b, thereby liberating two H_2O molecules (see Eq. (5.2) above). A reaction enthalpy of −0.33 eV for the relaxed structure from model B21, was calculated according to the equation listed in Table 9. This enthalpy is lower than its T22 counterpart by 0.46 eV: this implies that the proposed reaction is likely to favor the products. Although the VPA molecule is probably slightly less constrained in the bidentate configuration, it should be kept in mind that we did not remove a surface H ion to liberate an integral number of H_2O molecules as we did for model T22. In addition, the free leg of the VPA fragment (P═O bond) could participate in hydrogen bonding with the oxide surface. These are possible reasons why the model B21 enthalpy is lower than that predicted for T22. The P–O bond distances listed in Table 10 show that the two surface bonds have the same distance as their counterparts in model T22 (see Table 8). However, the free leg of the VPA fragment base in the relaxed structure had a 1.51 Å distance between the P and O ions, which was shorter than each of the

[4] The only commonality between bidentate model B21 and tridentate model T21 rests with the fact that both were bound at site 2. Otherwise the two models are unrelated. The same comments apply to tridentate, bidentate, and unidentate models with similar suffices (e.g. T21, B21, U21).

Table 9
Bidentate reaction enthalpy equations

Model	H_R
B21	$H_R = (H_{BP} + 2H_{H_2O}) - H_{\alpha\text{-}Al_2O_3(0001)} - H_{VPA}$
B22	$H_R = (H^*_{BP} + H_{H_2O})^a - H_{\alpha\text{-}Al_2O_3(0001)} - H_{VPA}$

[a] H^*_{BP} includes adsorbed H_2O molecule.

Table 10
Bidentate reaction enthalpies

Model	VPA conformation	H_R (eV) $H_{H_2O} = -14.71$ eV (from Eq. (5.1))	P–O (Å) Relaxed
B21	180°	−0.33	1.57[a], 1.60[a], 1.51
B22	180°	+0.01	1.56[a], 1.59[a], 1.51

[a] Denotes VPA phosphorus ion bound to oxide surface oxygen ion.

three bond distances measured for model T22. This distance was close to that of the 1.47 Å, P=O distance (see Table 2) for the isolated VPA molecule.

It was of interest to examine the effect of an adsorbed H_2O molecule on the binding energetics of model B21 since VPA is likely to react in the presence of moisture (and hence model B21 is certainly far from the reality of practical application). For this reason, we constructed model B22 using the starting geometry for B21, but included a single H_2O molecule near the center site 1. There were obviously many different possible starting orientations of the H_2O molecule and hence we had to limit our efforts by making a reasonable starting guess for its position on the surface. However, our previous calculations for H_2O adsorption gave us confidence that we had a near optimal placement of the H_2O molecule on the relaxed surface. The relaxed geometry for model B22 is shown in Fig. 13. The reaction enthalpy for model B22 was calculated according to the equation listed in Table 9. Table 10 lists the calculated reaction enthalpy as +0.01 eV. A comparison with the results for model B21 shows that inclusion of the adsorbed H_2O molecule actually raised the reaction enthalpy. We suspect that there was an electrostatic effect between the H_2O molecule and the bound VPA fragment that contributed to a decrease in the reaction energy. A comparison of the reaction enthalpies computed for models B22 and T23, both of which involved an adsorbed H_2O molecule due to VPA reaction with the oxide surface, shows that the tridentate coordination led to lower reaction enthalpy than that for its bidentate counterpart.

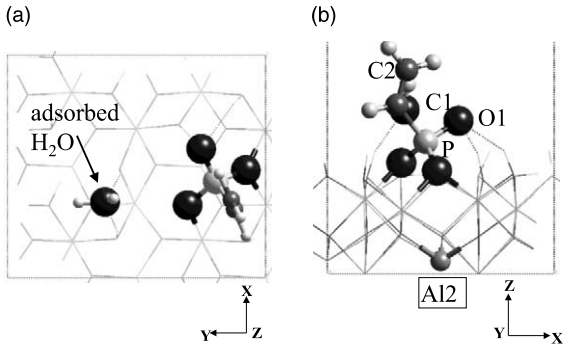

Fig. 13. Model B22, relaxed geometry: (a) view down [0 0 0 $\bar{1}$], (b) along Y-direction.

5.4. Unidentate models

Three unidentate models were constructed at site 2 in Fig. 6b. Two reaction enthalpy calculations were considered, and the corresponding equations for these reactions are listed in Table 11. Note that structures for each of the unidentate models were shifted along the Y-axis designated in the corresponding figures so as to centrally position the relaxed components.

The starting geometry for model U21 was constructed by assuming that leg O2H2 in the VPA tripodal base of Fig. 3 reacted with a single hydroxyl bridge at site 2 on α-Al_2O_3(0 0 0 1) in Fig. 6b. The VPA fragment was then manually rotated so that legs P=O and O3H1 were nearly parallel

Table 11
Unidentate reaction enthalpy equations

Model(s)	H_R
U21,U22	$H_R = (H_{BP} + H_{H_2O}) - H_{\alpha-Al_2O_3(0001)} - H_{VPA}$
U23	$H_R = H^{*}_{BP}{}^{a} - H_{\alpha\text{-}Al_2O_3(0001)} - H_{VPA}$

[a] H^*_{BP} includes adsorbed H_2O molecule.

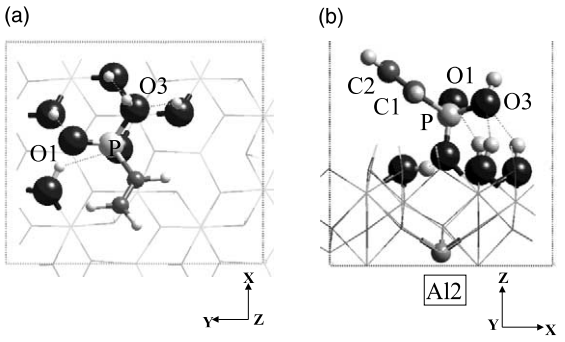

Fig. 14. Model U21, relaxed geometry: (a) view down [0 0 0 $\bar{1}$], (b) along *Y*-direction.

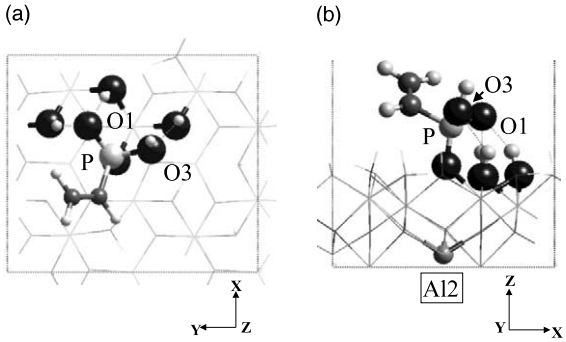

Fig. 15. Model U22, relaxed geometry: (a) view down [0 0 0 $\bar{1}$], (b) along *Y*-direction.

with the surface plane, and the resulting structure was then relaxed. A single H_2O molecule, which was not included in the cell with the bound VPA fragment, was liberated in the reaction.

Fig. 14 show two views of the relaxed structure corresponding to model U21. The calculated reaction enthalpy, which is listed in Table 12, was +0.29 eV. Even though one leg of the VPA fragment appears to be engaging in hydrogen bonding with the surface (see Fig. 14b), the calculated reaction enthalpy implies that the proposed geometry is unlikely to be energetically favorable. Note that the three P–O bond distances are listed in Table 12. One of these, i.e., 1.49 Å, is close to the P=O distance of 1.47 Å in the VPA tripodal base (see Table 2).

The starting geometry for model U22 was taken from model U21. This model was an experiment of sorts in that we rotated the VPA fragment clockwise through 90° about [0 0 0 1] prior to relaxing the resulting geometry. Our interest here was to determine if there might be an energetically more favorable unidentate coordination. The rotation of the VPA fragment placed O1 midway between two hydroxyl bridges as shown in the relaxed "top–down" view in Fig. 15a. The calculated reaction enthalpy in Table 12, which was +0.29 eV, indicates that the rotation produced no change in the enthalpy. The P–O bond distances for model U22 differ insignificantly from those for model U21.

As a final consideration, it was of interest to explore the energetics of VPA reaction through the phosphoryl oxygen, O1 in Fig. 3. This was the purpose of model U23, in which the VPA fragment was assumed to react with a single hydroxyl bridge at site 2, thereby displacing the bridge through reaction with O1, and resulting in adsorption of the OH group at site 3 in Fig. 6b. [5] For the starting geometry, the liberated hydroxyl group was placed directly above a surface hydroxyl group at site 3.

Two views of the relaxed geometry corresponding to model U23 are shown in Fig. 16, along with several surface hydroxyls that we suspected were involved in hydrogen bonding with the VPA fragment. During the relaxation, we assumed that the adsorbed hydroxyl group reacted with leg O2H2 in the VPA fragment and formed an adsorbed H_2O molecule, which is shown in both Fig. 16a and b. The VPA fragment remained bound to the surface after restoring the phosphoryl

Table 12
Unidentate reaction enthalpies

Model	VPA conformation	H_R (eV) $H_{H_2O} = -14.71$ eV (from Eq. (5.1))	P–O (Å) Relaxed
U21	180°	+0.29	1.54[a], 1.65[b], 1.49
U22	180°	+0.29	1.54[a], 1.63[b], 1.51
U23	180°	−0.10	1.56[a], 1.59[b], 1.51

[a] Denotes VPA phosphorus ion bound to oxide surface oxygen ion.

[b] Denotes VPA phosphorus ion bound to a free hydroxyl leg.

[5] A fundamental difference between U22 and U23 is that for the former model we assume that H_2O binds to a bare surface, but in the latter, we allow H_2O to interact with the VPA fragment.

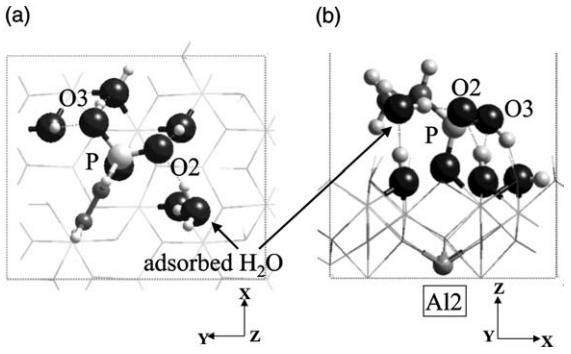

Fig. 16. Model U23, relaxed geometry: (a) view down [0 0 0 $\bar{1}$], (b) along Y-direction.

oxygen at what was originally O2H2 in Fig. 3. This is supported by the 1.51 Å distance reported for model U23 in Table 12. This led to the lowest reaction enthalpy of the three unidentate models considered, i.e. −0.10 eV, as listed in Table 11. Note that numerous hydrogen bonds also contributed to the decrease in reaction enthalpy, including a likely hydrogen bond between O2 in Fig. 16b and the H_2O molecule. Hence, the VPA molecule is likely to initially react with α-Al_2O_3(0 0 0 1) through one of the hydroxyl legs in its tripodal base group, as suggested by Fig. 2b. Water formation from an adsorbed hydroxyl group contributed to a decrease in the reaction enthalpy, a result which follows (in at least a qualitative sense) the energetics associated with model T23, but certainly does not follow the energetics associated with B22 (although the initial model B22 started with an adsorbed H_2O molecule, but the initial models T23 and U23 started with adsorbed OH groups that subsequently became H_2O molecules during the relaxation). The differences are due largely to the formation of H_2O from an adsorbed OH group, the position of adsorbed water molecule on the surface, unbound VPA tripodal base components, and any resulting hydrogen bonds.

Some comments on the entropy contributions from the VPA and H_2O molecules to the reaction energetics are warranted. In Ref. [62], $H^{\text{isolated}}_{H_2O}$ was corrected with handbook data in order to gain good agreement between DFT calculations of the phase stability and structure of spinel-based transition aluminas and available experimental data. Following Ref. [62], we write the free energy of formation for an H_2O molecule, $G^{\text{liquid}}_{H_2O}$, as follows:

$$G^{\text{liquid}}_{H_2O} = H^{\text{isolated}}_{H_2O} + H^{\text{liquid–gas}}_{H_2O} - TS^{\text{liquid}}_{H_2O} \tag{5.5}$$

where $H^{\text{isolated}}_{H_2O}$ is the GGA-predicted enthalpy of an isolated H_2O molecule, $H^{\text{liquid–gas}}_{H_2O}$ and $S^{\text{liquid}}_{H_2O}$ are the enthalpic and entropic contributions, respectively.

For $T = 298$ K, $H^{\text{liquid–gas}}_{H_2O} = -0.46$ eV and $TS = 0.21$ eV [50]. This gives $G^{\text{liquid}}_{H_2O} = -14.96$ eV. The above correction will therefore always result in a more favorable estimate of the reaction enthalpy (for any given coordination) than that due to Eq. (5.1) if in fact we neglect the entropic contribution from the VPA molecule. At present, however, we have no entropy data for the VPA molecule. However, it is likely that the entropy of an adsorbing VPA molecule is approximately the same as that for a single H_2O molecule (although the two quantities differ in sign). Hence, based upon this qualitative argument, the tridentate coordination will be most favorable, followed by the bidentate coordination.

6. Concluding remarks

Using first principles total energy calculations, we investigated the reaction energetics for VPA binding to an idealized α-Al_2O_3(0 0 0 1) surface. Since published results from IETS experiments implied a tridentate coordination following a condensation reaction between VPA and the oxide surface, we began our investigation by probing three different threefold sites on the surface for favorable VPA tridentate bonding. These sites were distinguished by the total distances between adjacent hydroxyl bridges in the relaxed surface and the proximity of an underlying Al ion in the oxide surface to the VPA phosphorus ion in the relaxed structure. We also constructed bidentate and unidentate coordinations in order to make qualitative comparisons between the reaction energetics calculated for each coordination.

The major conclusions from this work are: (a) the tridentate coordination had the most negative reaction enthalpy, and the unidentate coordination had the least negative reaction enthalpy; (b)

VPA molecule binding to the oxide surface was site sensitive and depended upon the geometry of the surface and the distance of the underlying Al ion directly beneath the centroid of the site; (c) for the two VPA geometries that we examined, the angular orientation of the hydrocarbon tail relative to the bound tripodal base was found to insignificantly effect the tridentate reaction enthalpies; (d) the character of the P–O bonds that anchor the VPA fragment to the oxide surface are primarily ionic with a small degree of covalency (i.e. the ELF lobes on the O ions are directed towards the P ion). No significant changes occurred in the bonding character of the vinyl group.

Clearly, adsorbed water molecule placement offers a large number of possible structures, and we explored only a very limited number of these. It would be of interest to return to the most energetically favorable structures predicted in this work, and systematically move the H_2O molecule around the VPA fragment (i.e. from site-to-site) and subsequently calculate the reaction energetics. This would involve a refinement to the present work that would lead to more definitive conclusions about the role of adsorbed water in the different reaction coordinations, especially as a means through which to confirm the hydrolytic stability of the tridentate coordination. In addition, it would be of interest to more efficiently quantify electrostatic effects between the VPA phosphorus ion and underlying Al ions in the oxide surface.

A variety of metallic alloying agents are used in aluminum alloy manufacturing. The most common of these are manganese, magnesium, zinc, and copper. In addition, iron often appears as an impurity. It would be interesting to repeat the selected calculations presented in this work on different oxide surfaces containing one or more these ions. For example, cubic MgO is a common component on aluminum alloy surfaces and it would be of interest to examine VPA reaction energetics on an MgO surface. The hydroxylated MgO(1 1 1) displays a three fold site geometry that might be conducive to the tridentate coordination. Unlike the α-Al_2O_3(0 0 0 1) surface considered in this work, however, the hydroxylated MgO(1 1 1) surface contains only one site geometry. Vinyl phosphonic reaction with additional oxide structures, such as γ-$Al(OH)_3$, α-$Al(OH)_3$, α-AlOOH, α-AlOOH and γ-Al_2O_3, should also be studied.

Acknowledgements

The authors wish to express their sincerest thanks to Dr. Ken Hass of the Ford Research Laboratory for his review of the manuscript and many helpful suggestions. The authors also wish to acknowledge Georg Kresse of the University of Vienna for use of the VASP code, and for his technical assistance with the code. Financial support for D.J. Siegel, H. Yu, and J.A. Adams was provided by the National Science Foundation Division of Materials Research under grant DMR9619353. The computational resources of the National Computational Science Alliance (NCSA) at the University of Illinois at Urban-Champaign are gratefully acknowledged.

References

[1] R. Coast, M. Pikus, P.N. Henriksen, G.A. Nitowski, J. Adhes. Sci. 2 (1996) 101.
[2] G.A. Nitowski, Ph.D. Thesis, Virginia Polytechnic State University, 1998.
[3] K. Wefers C. Misra. Oxides and Hydroxides of Aluminum, Alcoa Technical Paper No. 19, Revised. Alcoa Technical Center, Alcoa, PA., 1987.
[4] K. Wefers, G.A. Nitowski, L.F. Wieserman, U.S. Patent 5,126,210 (1992).
[5] R.T. Foley, Corrosion 42 (1986) 277.
[6] J.R. Davis, Sr., Metals Handbook, ninth ed., ASM International, Ohio, 1987, p. 583.
[7] C.-T. Lin, U.S. Patent 5,322,870 (1994).
[8] M.R. Bothwell, R.L. Kane, H.P. Godard, W.B. Jepson, R.L. Kane, The Corrosion of Light Metals, Wiley, New York, 1967.
[9] B.R.A. Neves, D.N. Leonard, M.E. Salmon, P.E. Russell, Nanotechnology 10 (1999) 399.
[10] P.K. Hansma, in: P.K. Hansma (Ed.), Tunneling Spectroscopy, Plenum Press, New York, 1982.
[11] R.D. Ramsier, P.N. Henriksen, A.N. Gent, Surf. Sci. 203 (1988) 72.
[12] F.A. Cotton G. Wilkinson, Advanced Inorganic Chemistry, fifth ed., Wiley-Interscience, New York, 1988.
[13] V.E. Henrich, P.A. Cox, The Surface Science of Metal Oxides, Cambridge University Press, New York, 1994.

[14] C. Noguera, Physics and Chemistry at Oxide Surfaces, Cambridge University Press, New York, 1996.
[15] M. Scheffler, C. Stampfl, in: K. Horn, M. Scheffler (Eds.), Handbook of Surface Science, Elsevier, Amsterdam, 2000.
[16] J.E. Hatch, Aluminum. Properties Physical Metallurgy, American Society for Metals, Metals Park, 1984.
[17] W. Kohn, L. Sham, Phys. Rev. 140 (1965) A1133.
[18] R.O. Jones O. Gunnarsson, Rev. Mod. Phys. 61 (1989) 689.
[19] R. Car, M. Parinello, Phys. Rev. Lett. 55 (1985) 2471.
[20] M.C. Payne, M.P. Teter, D.C. Allan, T.A. Arias, J.D. Joannopoulos, Rev. Mod. Phys. 64 (1992) 1045.
[21] G. Kresse, J. Hafner, Phys. Rev. B. 48 (1993) 13115.
[22] G. Kresse, J. Furthmüller, Comput. Mat. Sci. 6 (1996) 15.
[23] G. Kresse, J. Furthmüller, Phys. Rev. B. 54 (1996) 11169.
[24] D. Vanderbilt, Phys. Rev. B 41 (1990) 7892.
[25] P.E. Blöchl, Phys. Rev. B 50 (1994) 17953.
[26] G. Kresse, D. Joubert, Phys. Rev. B 59 (1999) 1758.
[27] J. Fürthmuller, P. Käckell, F. Bechstedt, G. Kresse, Phys. Rev. B 61 (2000) 4576.
[28] J. Emsley, The Elements, second ed., Clarendon Press, London, 1992.
[29] H.J. Monkhorst, J.D. Pack, Phys. Rev. B 13 (1976) 5188.
[30] P. Pulay, Chem. Phys. Lett. 73 (1980) 393.
[31] J.P. Perdew, Y. Wang, Phys. Rev. B 46 (1992) 6671.
[32] J.P. Perdew, J.A. Chevary, S.H. Vosko, K.A. Jackson, M.R. Pederson, D.J. Singh, C. Fiolhais, Phys. Rev. B 46 (1992) 6671.
[33] R.T. Morrison R.N. Boyd, Organic Chemistry, third ed., Allyn Bacon, Boston, 1973.
[34] A. Hernandez-Laguna, C.I. Sainz-Diaz, Y.G. Smeyers, J.L.G. de Paz, J.L.G., E. Galvez-Ruano, J. Phys. Chem. 98 (1994) 1109.
[35] A.D. Becke, K.E. Edgecombe, J. Chem. Phys. 92 (1990) 5397.
[36] A. Savin, R. Nesper, S. Wengert, T.F. Fässler, Angew. Chem. Int. Ed. Engl. 36 (1997) 1808.
[37] B. Silvi, A. Savin, Nature 371 (1994) 683.
[38] J.K. Burdett, T.A. McCormick, J. Phys. Chem. A 102 (1998) 6366.
[39] L. De Santis, R. Resta, Surf. Sci. 450 (2000) 126.
[40] P. Lamparter, R. Kniep, Physica B 234-36 (1997) 234.
[41] X.Y. Liu, P.P. Ohotnicky, J.B. Adams, C.L. Rohrer, R.W. Hyland Jr., Surf. Sci. 373 (1997) 357.
[42] K. Wefers, Aluminum (Düsseldorf) 57 (1981) 722.
[43] K. Shimizu, G.M. Brown, K. Kobayashi, P. Skeldon, G.E. Thompson, G.C. Wood, Corros. Sci. 40 (1998) 557.
[44] S.-D. Mo, W.Y. Ching, Phys. Rev. B 57 (1998) 15219.
[45] P. Guenard, G. Renaud, A. Barbier, M. Gautier-Soyer, Surf. Rev. Lett. 5 (1997) 321.
[46] F.D. Murnaghan, Proc. Nat. Acad. Sci. 30 (1944) 244.
[47] J.C. Boettger, Phys. Rev. B 55 (1997) 750.
[48] B.G. Hyde, S. Andersson, Inorganic Crystal Structures, Wiley, New York, 1989.
[49] P. Richet, J. Xy, H.K. Mao, Phys. Chem. Miner. 16 (1988) 207.
[50] CRC Handbook of Chemistry Physics, 76th ed., CRC Press, Boca Raton, 1995.
[51] Y.S. Touloukian, R.K. Kirby, R.E. Taylor, T.Y.R. Lee, Thermophysical Properties of Matter, vol. 13, Plenum, New York, 1974, p. 176.
[52] H. d'Amour, D. Schiferl, J. Appl. Phys. 49 (1978) 4411.
[53] L.E. Finger, R.M. Hazen, J. Appl. Phys. 49 (1978) 5823.
[54] M.A. Nygren, D.H. Gay, C.R.A. Catlow, Surf. Sci. 380 (1997) 113.
[55] C. Verdozzi, D.R. Jennison, P.A. Schultz, M.P. Sears, Phys. Rev. Lett. (1999) 799.
[56] D.J. Siegel, L.G. Hector Jr., J.B. Adams, Phys. Rev. B, in preparation.
[57] J.C. Boettger, Phys. Rev. B. 49 (1994) 16798.
[58] K.C. Hass, W.F. Schneider, A. Curioni, W. Andreoni, Science 282 (1998) 265.
[59] R.D. Felice, J.E. Northrup, Phys. Rev. B 60 (1999) 16287.
[60] P.J. Eng, T.P. Trainor, G.E. Brown, G.A. Waychunas, M. Newville, S.R. Sutton, R. Stephen, M.L. Rivers, Science 288 (2000) 1029.
[61] G.A. Jeffrey, An Introduction to Hydrogen Bonding, Oxford University Press, New York, 1997.
[62] C. Wolverton, K. Hass, Phys. Rev. B, in press.